

# Optical Strategies for Sensing Neuronal Voltage using Quantum Dots and Other Semiconductor Nanocrystals

Jesse D. Marshall<sup>†</sup> and Mark J. Schnitzer<sup>†,‡, §</sup>

<sup>†</sup>James H. Clark Center, <sup>‡</sup>Howard Hughes Medical Institute, <sup>§</sup>CNC Program  
Stanford University, Stanford, CA 94305

Correspondence: jessem1@stanford.edu, mschnitz@stanford.edu

## SUPPLEMENTARY INFORMATION

### Supplementary Figures

Figure S1

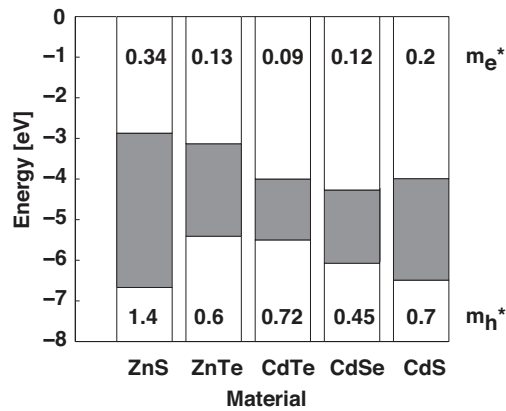
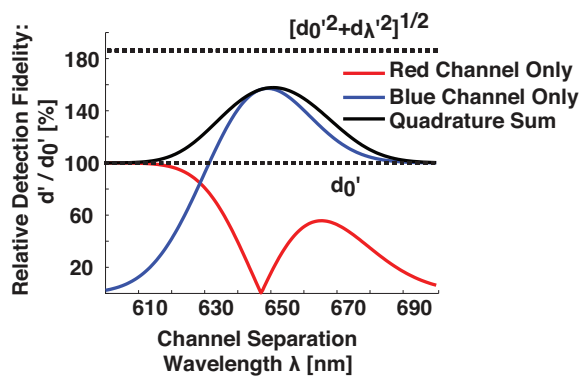
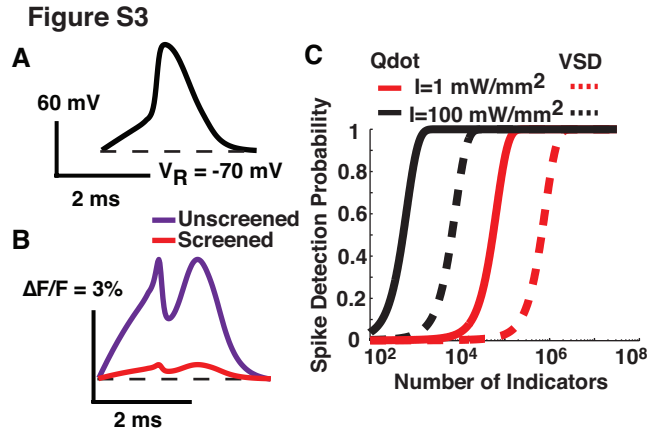


Figure S2





### Supplementary Figure Captions:

**Figure S1.** | Valence and conduction band offsets and effective masses for different II-VI semiconductors, relative to vacuum.<sup>1,2</sup> The gray areas represent the band gaps.

**Figure S2.** | The use of two fluorescence color channels can improve the spike detection fidelity of voltage measurements performed using qdots. Here the emission pathway is separated into two color channels, denoted red and blue, which respectively collect emission photons above and below a single variable wavelength  $\lambda$  (Fig. 4 F). The red and blue solid lines show the spike detection fidelity values obtained by using the two channels individually. The solid black line shows the quadrature sum of the values from the two channels. For comparison, the lower dashed line shows the spike detection fidelity obtained when all emission photons are detected within a single channel, regardless of wavelength. The upper dashed line shows the theoretical limit on  $d'$  obtained using measurements of both fluorescence intensity and emission spectrum, e.g. with a spectrometer.

**Figure S3.** | Unscreened qdots are superior single-photon spike detectors than existing voltage-sensitive dyes. (A) Simulated action potential in a neocortical neuron and (B) the corresponding fluorescence changes in a CdTe qdot of 4 nm radius screened and unscreened by the membrane. Note that qdot fluorescence depends on the absolute field strength. (C) The spike detection probability  $P_D$  for an unscreened qdot and voltage-sensitive dyes (VSD) in widefield epi-fluorescence imaging as a function of the excitation intensity and number of indicators, assuming a fixed false positive rate  $P_F=0.1\%$ .

## SI TEXT

### VOLTAGE-SENSITIVITY OF QUANTUM DOT EIGENSTATES

The absorption of a photon in a semiconductor excites an electron from the valence band to the conduction band, leaving a positively charged hole. These charge carriers form a bound state, called an exciton, due to the Coulomb interaction. Light is reemitted upon the recombination of the carriers, producing a photon of energy  $E_\gamma = E_g + E_{\text{ex}}$ , where  $E_g$  is the bandgap energy and  $E_{\text{ex}}$  is the energy of the exciton.

Applying the effective mass and envelope approximations to the bulk (Bloch) wavefunctions of the electron and hole yields approximate wavefunctions for the carriers inside a nanocrystal.<sup>3-5</sup> These approximations separate the wavefunctions into an envelope wavefunction that varies smoothly over the crystal and a unit cell wavefunction that is periodic in the crystal lattice. The following quantum mechanical Hamiltonian governs this system:

$$H = \frac{\hbar^2}{2m_e^*} \nabla_e^2 + \frac{\hbar^2}{2m_h^*} \nabla_h^2 + \frac{e^2}{4\pi\epsilon_s |\mathbf{r}_e - \mathbf{r}_h|} + V_{\text{conf}} \quad (1)$$

Here  $\nabla_e$  ( $\nabla_h$ ) denotes the  $\nabla$  operator with respect to the electron (hole) position,  $r_e$  ( $r_h$ ),  $\epsilon_s$  is the static dielectric constant of the semiconductor, and  $V_{\text{conf}}$  is the potential created by the band offset between the qdot core and its shell or the surrounding medium. Here we assume the band offset is infinite. We note that corrections will only enhance the polarizability of the wavefunction, and hence the qdot's voltage-sensitivity.

The envelope wavefunction determines the nanocrystal's voltage-sensitivity. For particles confined in a spherical volume by infinite well boundary conditions the envelope eigenstates are:<sup>4</sup>

$$\psi_{nlm} = A_{nlm} j_l \left( k_n l \frac{r}{R} \right) Y_{lm}(\theta, \phi) = Y_{lm}(\theta, \phi) \frac{\sqrt{2} J_{l+1/2}(k_{nl} r / R)}{R \sqrt{r} J_{l+3/2}(k_{nl} R)} \quad (2)$$

Here the  $J_l$  and  $j_l$  are the normal and spherical Bessel functions of the first kind,  $k_{nl}$  is the  $n^{\text{th}}$  root of  $J_l$ ,  $R$  is the sphere's radius,  $A_{nlm}$  is a normalization constant and the  $Y_{lm}$  are spherical harmonics. These states have energies  $E_{nlm} = \hbar^2 k_{nl}^2 / 2m_h^* R^2$ . Ignoring the Coulomb interaction between the electron-hole pair, we can apply perturbation theory to calculate the mixing induced by the electric field inside the dot,  $E_z$ , for both the electron and hole states. Here the states have been relabeled with a single index for clarity. The odd parity of the perturbation resulting from  $V_E = -eE_z z$  implies the lowest-order corrections to the ground state are first-order wavefunction shifts and second-order energy shifts:

$$E_n^{(2)} = \sum_{m \neq n} \frac{|\langle \psi_n | V_E | \psi_m \rangle|^2}{E_n - E_m} \propto \frac{-e^2 E_z^2 R^4}{\hbar^2 / 2m_h^*} \quad (3)$$

$$|\psi_n^{(1)}\rangle = \sum_{m \neq n} |\psi_m\rangle \frac{|\langle \psi_n | V_E | \psi_m \rangle|}{E_n - E_m} \propto \frac{-eE_z R^3}{\hbar^2 / 2m_h^*} |\psi_{110}\rangle \quad (4)$$

where the proportionality is obtained by only considering mixing of the ground state with the  $|\psi_{110}\rangle$  state. The strength of the perturbation is proportional to the effective mass. Since electron effective masses are smaller than hole effective masses for II-VI

semiconductors, the electron wavefunction  $|\psi_e\rangle$  will be less perturbed than the hole. The same is true for the Coulomb interaction, so by approximating the electron wavefunction as unperturbed  $|\psi_e\rangle = |\psi_{100}\rangle$ , the hole perturbation becomes:<sup>5</sup>

$$V_c(r_h) = \langle \psi_e | \frac{e^2}{4\pi\epsilon_s |\mathbf{r}_e - \mathbf{r}_h|} | \psi_e \rangle = \frac{e^2}{2\pi\epsilon_s R} \int_0^1 dr_e \sin(\pi r_e)^2 \left[ \frac{\theta(r_h - r_e)}{r_h} - \frac{\theta(r_e - r_h)}{r_e} \right], \quad (5)$$

where  $\theta$  is the Heaviside step function. The interaction has spherical symmetry, so the first hole states mixed are the  $|\psi_{100}\rangle$  and  $|\psi_{200}\rangle$  states. Because of the large energy separation between the states, the mixing is small and the perturbative scaling laws are relatively unaffected, although there is a modification to the overall ground state energy. Power law least squares fits made to the cross-sections of Fig. 2A and B for  $R = 4$  nm and  $E_z = 10$  mV/nm yields:  $\Delta E \propto E_z^{1.96 \pm 0.01} R^{3.71 \pm 0.07}$  and  $\Delta \tau \propto E_z^{1.93 \pm 0.02} R^{5.41 \pm 0.15}$ .

## QUANTUM DOT RADIATIVE DYNAMICS

Here we calculate how modulation of the radiative lifetime of semiconductor nanocrystals produces changes in the rate of fluorescence emission. We model the fluorescence dynamics of nanocrystals as those of a two-state system, assuming rate constants for n-photon excitation from the ground state,  $k_n = \sigma_n [I / (\hbar\omega)]^n$ , and radiative and non-radiative decay from the excited state  $k_r$  and  $k_{nr}$ , respectively. This produces an overall rate constant for decay  $k_d = k_r + k_{nr}$  and quantum yield  $\Phi_F = k_r/k_d$ . In solution, these rates of decay can be variable and dependent on local environmental conditions and excitation intensity,<sup>6, 7</sup> producing dynamics with fluctuating multi-exponential behavior. However, we are interested in fluorescence measurements that probe the average decay rate and its modulation averaged over a large number of indicators, justifying the two-state approximation.

By integrating the rate equations directly for the case of continuous excitation of  $N$  emitters, we find that a steady state fluorescence rate  $F_{CW}$  is reached within several tens of nanoseconds:

$$F_{CW} = N \frac{k_a k_r}{k_a + k_d} = N \frac{k_r}{1 + k_r / \Phi_F k_a}. \quad (6)$$

In this model, having a low quantum yield improves sensitivity to fluorescence changes for small shifts  $\Delta \tau_r$ :

$$\frac{\Delta F_{CW}}{F_{CW}} = \frac{\partial F_{CW}}{\partial \tau_r} \Delta \tau_r = -N(1 - \Phi_F) \frac{\Delta \tau_r}{\tau_r}. \quad (7)$$

We also consider systems with pulsed laser excitation with repetition rate  $\nu_p$  and laser pulse width  $\tau_p$ . The population reaches steady state equilibrium within several pulses. The steady state fluorescence rate,  $F_P$ , is derived by directly by balancing the number of fluorophores excited per pulse with the number that decays, producing fluorescence rates:

$$F_p = N v_p \Phi_F \frac{(e^{k_a \tau_p} - 1)(1 - e^{-k_d/v_p})}{e^{k_a \tau_p} - e^{-k_d/v_p}} \quad (8)$$

For small shifts  $\Delta\tau_r$ , we can readily calculate the size of shifts in the fluorescence rate  $F_p$  in the case of complete pulse saturation,  $I \rightarrow \infty$ :

$$\frac{\Delta F_p}{F_p} = -N v_p \Phi_F \frac{\Delta\tau_r}{\tau_r} \left[ (1 - \Phi_F) + \frac{k_d/v_p e^{-k_d/v_p}}{1 - e^{-k_r/\tau_p}} \right] > \frac{\Delta F_{CW}}{F_{CW}} \quad (9)$$

### DIELECTRIC SCREENING IN A TRANSMEMBRANE QDOT:

Hydrocarbon chains composing the majority of the bilipid layer have a dielectric constant  $\epsilon_L \sim 2$ ,<sup>8</sup> close to the value for bulk liquid hydrocarbons. For the relatively large qdot sizes considered here, the qdot static dielectric constant approaches its bulk value,<sup>9</sup> which for II-VI nanocrystals is  $\epsilon_s \sim 10$ .<sup>1</sup> We consider a bilipid layer of length  $2d_1$  with a quantum dot of diameter  $d_2$ . In the limit of homogenous polarization, a charge density  $\sigma$  on one side of the membrane will produce transverse fields  $\bar{E}_i = \sigma/\epsilon_i$ ,  $i \in \{1, 2\}$  across the bilipid layer and membrane, respectively. The transmembrane potential,  $V$  is fixed, which determines the value of the charge density:

$$\sigma = \frac{V}{2d_1/\epsilon_1 + d_2/\epsilon_2} \quad (10)$$

At the peak membrane thickness, this produces a screened field inside the qdot of strength:

$$\bar{E}_2 = \frac{V}{2d_1\epsilon_2/\epsilon_1 + d_2} \quad (11)$$

For a 4 nm thick membrane and an embedded qdot of radius 4 nm, the field inside is reduced to 30% of its unscreened strength.

This model provides an estimate of the capacitive loading of the membrane due to quantum dots. Assuming a uniform field across the dot, the ratio of membrane surface charge with and without a qdot  $\sigma/\sigma_0$  is  $1 + d_2\epsilon_1/2d_1\epsilon_2$  in the screened case and  $d_2\epsilon_1/2d_1\epsilon_2$  in the unscreened case. For the thicknesses assumed above,  $\sigma/\sigma_0 \sim 150\%$  in the screened case and  $\sim 50\%$  in the unscreened case. Assuming a qdot surface density of  $\sim 1/100 \text{ nm}^{-2}$ , the overall capacitive change is then  $< 1\%$ .

### SPIKE DISCRIMINABILITY USING VOLTAGE INDICATORS

As above, given a fluorescence intensity trace consisting of  $K$  time frames,  $F(t_i)_{i=1}^K = F(t)$ , we wish to test the hypothesis  $H_1$ , that there is an optical waveform of a spike, subject to Poisson-distributed shot noise with mean  $F(t) = S(t)$ . The null hypothesis  $H_0$ , is that the fluorescence distribution has mean equal to the baseline fluorescence rate of the system,  $F_0$ . We assume a large number of photons are collected in each frame, so that the distributions of photons collected under each hypothesis are approximately Gaussian, and

that  $F_0 \gg \Delta F_i \equiv S(t_i) - F_0$  so that the variances are approximately equal. The general Poisson case is derived in the references.<sup>10</sup> The log-likelihood of fluorescence trace under the two hypotheses is:

$$L(F(t_i)) = \log \frac{P(F(t) | H_1)}{P(F(t) | H_0)} = \sum_{i=1}^K \frac{S(t_i) - F_0}{F_0} \left( F(t_i) - \frac{S(t_i) + F_0}{2} \right) \quad (12)$$

We can create a decision rule,  $\delta(F(t))$ , that discriminates between the two hypotheses based on the value of the log-likelihood ratio:

$$\delta(F(t)) = \begin{cases} H_1 & L(F(t)) > \log(C) \\ H_0 & L(F(t)) \leq \log(C) \end{cases} \quad (13)$$

Here  $\log(C)$  can also incorporate the constant term from eq. (17) above. The Neyman-Pearson lemma<sup>11</sup> ensures that for a fixed false positive rate  $F_p = P(L(F(t)) > \log(C) | H_0)$  for discrimination between the two hypotheses, the likelihood ratio test is the statistical test with the greatest detection rate  $F_d = P(L(F(t)) > \log(C) | H_1)$ . Because the  $F(t_i)$  are normally distributed under each hypothesis, and the distribution of the sum of two Gaussian-distributed variables, the log-likelihood ratio is normally distributed under each hypothesis, with mean and variance:

$$\mu_j = E(L(F) | H_j) = \sum_{i=1}^K \frac{(S(t_i) - F_0)}{F_0} E(F | H_j) \quad (14)$$

$$\sigma_j^2 = \text{var}(L(F) | H_j) = \sum_{i=1}^K \frac{(S(t_i) - F_0)^2}{F_0^2} \text{var}(F | H_j) = \sum_{i=1}^K \frac{(\Delta F_i)^2}{F_0} \quad (15)$$

where  $j \in [0,1]$ . Note that the log-likelihood has equal variance,  $\sigma_0^2$ , under the two hypotheses. We can write  $P_D$  in terms of  $P_F$ :

$$P_D = \Phi\left(\frac{\mu_1 - \log(C)}{\sigma_0}\right) = \Phi\left(\Phi^{-1}(1 - P_F) + \frac{\mu_1 - \mu_0}{\sigma_0}\right), \quad (16)$$

and define  $d' \equiv (\mu_1 - \mu_0) / \sigma_0$ , as a single parameter defining the tradeoff between the two (eq. 3). Note that the  $d'$  values of multiple measurements sum in quadrature:

$$d'^2 = \frac{\left( \sum_{i=1}^K (\Delta F_i)^2 / F_0 \right)^2}{\sum_{i=1}^K (\Delta F_i)^2 / F_0} = \sum_{i=1}^K \frac{(\Delta F_i)^2}{F_0} \quad (17)$$

Measurements of indicator lifetime and wavelength are limited by the indicator's spectral width and variable lifetime. The former is described by a spectral line function,  $g(\lambda)$ , here assumed to be Gaussian with mean  $\bar{\lambda}_j$  and linewidth  $\bar{\sigma}_j$ ,  $j \in [0,1]$ . We

assume the fluorescence lifetime is exponentially distributed, with mean and standard deviation  $\bar{\tau}_j$ . For each time bin multiple independent measurements of wavelength and lifetime are performed, producing a time series of the mean wavelength  $\bar{\lambda}(t_i)$  or the mean lifetime  $\bar{\tau}(t_i)$ . The central limit theorem ensures that the probability distributions of  $\bar{\tau}(t_i)$  will be normally distributed with variance  $\bar{\tau}(t_i)/N_\gamma$  for large numbers of counts,  $N_\gamma$ . Recapitulation of the argument above for fluorescence measurements yields

$$d'^2 = \begin{cases} \sum_{i=1}^K N_\gamma \left( \frac{\bar{\tau}(t_i) - \bar{\tau}_0}{\bar{\tau}_0} \right)^2 \\ \sum_{i=1}^K N_\gamma \left( \frac{\bar{\lambda}(t_i) - \bar{\lambda}_0}{\bar{\sigma}_\lambda} \right)^2 \end{cases} \quad (18)$$

To first order in  $\Delta N_\gamma / N_\gamma$  these  $d'$ 's will be uncorrelated with measurements of fluorescence intensity.

For measurements of the spectral linewidth we are interested in measuring changes in a time series of linewidths  $\bar{\sigma}_j^2(t_i)$ . The probability density function of  $\bar{\sigma}_j^2(t_i)$  averaged over  $N_\gamma$  counts is a chi-squared distribution with variance  $2\bar{\sigma}_j^4(t_i)/N_\gamma$ , and again the central limit theorem guarantees convergence of the probability density function to a normal distribution in the high  $N_\gamma$  limit. The  $d'$  here is then:

$$d' = \sum_{i=1}^K \sqrt{N_\gamma} \left( \frac{\Delta \bar{\sigma}_i^2}{\sqrt{2\bar{\sigma}_i^2}} \right) \quad (19)$$

To calculate the enhancement in  $d'$  from the use of multiple color channels, separating the emitted fluorescence into distinct spectral bins indexed by pairs of wavelengths  $\{\lambda_i, \lambda_j\}$  produces a  $d'$  for a single frame:

$$d'^2 = \sum_{ij} N_\gamma \Delta_{ij} \left( 1 - \frac{\Delta_{ij} F'}{\Delta_{ij} F_0} \right) \quad (20)$$

Here  $\Delta_{ij} = \int_{\lambda_i}^{\lambda_j} g(\lambda) d\lambda$  are the different bins of the normalized emission profile,  $g(\lambda)$ , and primed quantities represent the corresponding quantity for the shifted line.

## SUPPLEMENTARY REFERENCES

1. Madelung, O., *Semiconductors: Data Handbook*. 3rd ed.; Springer: Berlin, 2004.

2. Zunger, A., Calculated Natural Band Offsets of All II–VI and III–V Semiconductors: Chemical Trends and the Role of Cation D Orbitals. *Appl Phys Lett* **1998**, *72*, 2011-2013.
3. Brus, L., A Simple Model for the Ionization Potential, Electron Affinity, and Aqueous Redox Potentials of Small Semiconductor Crystallites. *J. Chem. Phys.* **1983**, *79*, 5566.
4. Efros, A. L.; Efros, A., Interband Absorption of Light in a Semiconductor Sphere. *Sov. Phys. Semicond.* **1982**, *16*, 772-775.
5. Woggon, U., *Optical Properties of Semiconductor Quantum Dots*. Springer: New York, 1997.
6. Gómez, D.; Califano, M.; Mulvaney, P., Optical Properties of Single Semiconductor Nanocrystals. *Phys. Chem. Chem. Phys.* **2006**, *8*, 4989-5011.
7. Fisher, B.; Eisler, H.; Stott, N.; Bawendi, M., Emission Intensity Dependence and Single-Exponential Behavior in Single Colloidal Quantum Dot Fluorescence Lifetimes. *J. Phys. Chem. B* **2004**, *108*, 143-148.
8. Huang, W.; Levitt, D. G., Theoretical Calculation of the Dielectric Constant of a Bilayer Membrane. *Biophys. J.* **1977**, *17*, 111-28.
9. Wang, L.; Zunger, A., Pseudopotential Calculations of Nanoscale CdSe Quantum Dots. *Phys. Rev. B* **1996**, *53*, 9579-9582.
10. Wilt, B. A.; Fitzgerald, J. E.; Schnitzer, M. J., Photon Shot Noise Limits on Optical Detection of Neuronal Spikes and Estimation of Spike Timing. *Biophys. J.* **2013**, *104*, 51-62.
11. Poor, H. V., *An Introduction to Signal Detection and Estimation*. 2nd ed.; Springer-Verlag: New York, 1997.